Biosensors and Bioelectronics 25 (2010) 1622–1628

Contents lists available at ScienceDirect

Biosensors and Bioelectronics

journal homepage: www.elsevier.com/locate/bios

Electrochemical impedance biosensor with electrode pixels for precise counting of CD4$^+$ cells: A microchip for quantitative diagnosis of HIV infection status of AIDS patients

Xingqun Jiang*, Michael G. Spencer

School of Electrical and Computer Engineering, Cornell University, Ithaca, NY 14853, USA

ARTICLE INFO

Article history:
Received 2 October 2009
Received in revised form
25 November 2009
Accepted 25 November 2009
Available online 1 December 2009

Keywords:
CD4$^+$
HIV
AIDS
Biosensor
Microarray
Electrode

ABSTRACT

Oriented for the quantitative diagnosis of HIV infection status of AIDS patients, a cell biosensor based on electrochemical impedance spectroscopy has been developed for the precise counting of human CD4$^+$ cells. In this new biosensor, the sensing area was composed of densely packed working electrode pixels, each of which was comparable to a single CD4$^+$ cell in size. CD4$^+$ cells were captured on the chemically modified electrode pixels, and detected individually by monitoring the interfacial impedance changes on each independent pixel. The detection of a single cell was achieved by the "on" and "off" states of electrode pixel, depending on the cell capture status. The cell counting was digitalized by summing the electrode pixels in the "on" state (captured with a single cell). Compared with peer counting methods, the biosensor reported here was featured with a small device dimension, a minimal sample consumption, a finest detection resolution and a highest counting accuracy.

1. Introduction

Human immunodeficiency virus (HIV) is a lentivirus that leads to acquired immunodeficiency syndrome (AIDS) (Sepkowitz, 2001; Weiss, 1993). HIV primarily attacks CD4$^+$ T helper lymphocytes, macrophages, and dendritic cells in the human immune system (Alimonti et al., 2003). The progressive decline of the CD4$^+$ helper cells eventually leads to the loss of cell-mediated immunity, making the infected human bodies vulnerable to life-threatening opportunistic infections (Holmes et al., 2003). According to the recent report (Joint United Nations Programme on HIV/AIDS, 2008), 30–36 million people were living with HIV in 2007, together with 2.7 million new HIV infections and 2 million HIV-related deaths. Since its first recognition in 1981 (Gottlieb, 2006), HIV has been spread globally nowadays, especially in the developing countries in sub-Saharan Africa, where it accounted for 67% of the total population living with HIV and 75% of AIDS deaths in 2007.

The number of CD4$^+$ helper cells correlates with the status of the HIV infection. Clinically, an adult is considered to be healthy (no HIV infection) if the CD4$^+$ helper cells are more than 500 μl^{-1}. If the cells are below 200 μl^{-1}, the person is defined to have AIDS as his immune system is considered to be no longer strong enough to prevent opportunistic infections (Centers for Disease Control, 1993; Feldman, 2005). Therefore the quantification of the amount of CD4$^+$ helper cells is important for inspecting the HIV infection, diagnosing the infection stage of AIDS patients and determining the corresponding antiretroviral treatments (Department of Health and Human Services, 2005). The standard technique used for counting CD4$^+$ helper cells is flow cytometry (Landay et al., 1990). In flow cytometers, fluorescence tagged cells form a line and pass through a detection gate, scanned individually by a laser beam. The cell types are distinguished by the fluorescent chemicals that are attached to the cells through specific antigen–antibody recognitions. However, flow cytometry has its drawbacks such as sophisticated equipment, expensive costs and complicated operations. To meet the heavy needs of health care in resource-limited regions, affordable point-of-care diagnostic tools capable of quantifying CD4$^+$ cells with a minimum volume of whole blood sample are emphasized to be developed. Towards this direction, CD4$^+$ counting devices based on different detection methods have been reported in recent years. In the membrane-based microchip (Rodriguez et al., 2005), CD4$^+$ cells were harvested on porous polycarbonate membranes by filtering red blood cells through the membrane pores. Labeled with type-specific fluorescent antibodies, the CD4$^+$ cells were imaged under fluorescence microscope and were enu-

* Corresponding author at: School of Electrical and Computer Engineering, Cornell University, 252 Duffield Hall, Ithaca, NY 14853, USA.
E-mail addresses: xj22@cornell.edu (X. Jiang), spencer@ece.cornell.edu (M.G. Spencer).

0956-5663/$ – see front matter © 2009 Elsevier B.V. All rights reserved.
doi:10.1016/j.bios.2009.11.024

merated by digital image processing. In comparison with flow cytometry, however, this method exhibited relatively large counting errors. In the microfluidic devices (Cheng et al., 2007a,b), blood samples flowed through a 50-μm deep microfluidic channel that was modified with $CD4^+$ antibodies on the surface. The $CD4^+$ cells were separated from other types chromatographically and captured on the channel surface. The cell detection and counting was achieved by fluorescent labeling. However, the $CD4^+$ cells were more readily to be captured at the entrance of the microfluidic channel, instead of being uniformly distributed over the entire channel surface. In other microfluidic channels (Thorslund et al., 2008, 2007), polydimethylsiloxane (PDMS) was used as the primary material for the channel construction. Improvements in the optical methods included using quantum dots (Jokerst et al., 2008) as the fluorescent labeling marker, and using a MOSFET structure as a signal amplifier (Wang et al., 2008) in the $CD4^+$ cell detection.

Besides the optical detections, electrical method was also adopted in the $CD4^+$ counting devices. A cell biosensor based on electrochemical impedance spectroscopy (EIS) was developed (Mishra et al., 2005). The EIS method is generally advantageous in charactering interfacial phenomena with desired reliability and sensitivity. The biosensor was built with a three-electrode system, in which the working electrode was chemically modified with $CD4^+$ specific antibodies, being able to selectively capture $CD4^+$ cells. The electrochemical impedance spectrum between the working and the counter electrode was monitored upon the cell capture on the working electrode. The attachment of $CD4^+$ cells on the electrode surface caused an increase of impedance, especially in the low-frequency end. The impedance increase was correlated to the amount of $CD4^+$ cells captured on the working electrode.

These reported methods could potentially be integrated in the future practical devices. However, one common problem with these methods was that, the counting accuracy was not satisfactory yet. In other words, the counting results were subject to the dynamic range of the cell population. The counting error was generally proportional to the total cell number and could be large when the cell population was high. Therefore, counting cells with a consistent accuracy, independent of the dynamic range of the cell population, still remains as a challenge. In addition, for the reported devices, it was difficult to resolve the cells precisely when the total cells in the sample were low (e.g. <20 counts). However, for a point-of-care diagnostic tool designed for quantitatively evaluating the infection stage of AIDS patients, it is critical to have the capability of precisely counting sparse $CD4^+$ cells, because of two reasons: first, point-of-care tools are required to consume a minimal amount of blood samples; second, the $CD4^+$ cell concentration of AIDS patients is significantly lower than the normal value.

To address these issues, a novel EIS biosensor based on silicon substrate has been developed here with two important features: (1) a high counting accuracy, independent of the total cell counts; (2) a single-cell detection resolution. The three-electrode system was adopted in this new biosensor. Instead of being a single large working electrode, the sensing area consisted of an array of densely packed working electrode pixels, each of which had a size comparable to a single $CD4^+$ cell. Chemical modifications were applied on these electrode pixels, making them able to selectively capture $CD4^+$ cells. Each pixel was electrically independent, being able to capture and sense one $CD4^+$ cell only. The cell counting was simply achieved by summing the pixels whose surfaces were attached with single $CD4^+$ cells. With this sensor device, a precise counting of sparse $CD4^+$ cells has been successfully demonstrated by digitalizing the counting at single-cell resolution.

2. Experimental

2.1. Pixelated three-electrode system

4-inch double-side polished silicon wafers with an orientation [1 0 0] (Silicon Quest, Inc.) were cleaned in APM (NH_4OH:H_2O_2:H_2O = 1:1:6 at 70 °C) for 10 min and in HPM (HCl:H_2O_2:H_2O = 1:1:6 at 70 °C) for 10 min. A 300-nm thick low-stress Si_3N_4 film was deposited on the silicon substrate by LPCVD (DCS:NH_3 = 84 sccm:22 sccm, 200 mTorr, 800 °C). The adhesion promoter MicroPrime MP-P20 (Shin-Etsu MicroSi, Inc.) was spun on the wafers at 3000 rpm for 30 s, followed by spin coating the photoresist SPR955-CM 0.9 (MEGAPOSIT™) at 3000 rpm for 30 s. After baking at 90 °C for 90 s, the photoresist was exposed by autostep 200 mW cm^{-2} for 0.25 s. The wafers were then under the ammonia baking at 90 °C for 80 min, flood exposed for 60 s, and developed in 300 MIF (AZ Electronic Materials, Corp.) for 60 s. To remove the residual photoresist, the wafers were descumed by oxygen plasma cleaning at 80 °C for 1 min. The wafers were deposited with Cr (Research and PVD Material, Corp.) at 1 Å s^{-1} for 20 nm, followed by depositing Au (Research and PVD Material, Corp.) at 2 Å s^{-1} for 200 nm. The Au electrode pattern was finalized by soaking the wafers in the photoresist stripper 1165 (Rohm and Haas Electronic Materials, LLC) overnight.

After rinsing with dH_2O and drying under N_2 gas flow, the wafers were descumed by oxygen plasma cleaning at 80 °C for 60 s. A 2-μm thick PECVD Si_3N_4 film was deposited on the wafers as a passivation layer (IPE system, 200 °C for 130 min). To open the electrodes, the photoresist SPR955-CM 0.9 was spun on the wafers at 4000 rpm for 30 s and baked at 90 °C for 90 s. After exposing by autostep 200 mW cm^{-2} for 0.25 s, the photoresist was developed in 300 MIF for 1 min, rinsed with dH_2O and dried under N_2 gas flow. After descumed by oxygen plasma cleaning at 80 °C for 1 min, the wafers were under a CF_4 reactive ion etch for 25 min (chamber pressure: 40 mTorr, RF power: 150 W, CF_4 flow rate: 30 sccm) to remove the Si_3N_4 on the top of the electrodes. The fabrication schematic is shown in Fig. 1.

2.2. Cell culture

The cell lines used in the experiments were purchased from American Type Culture Collection (ATCC). J45.01 cells (ATTC: CRL-1990) were used as the mimic human $CD4^+$ T lymphocytes. $CD19^+$ Farage cells (ATCC: CRL-2630) were used in the control experiment. The two types of cells were cultured separately in the RPMI-1640 medium (ATCC) containing 10% fetal bovine serum (FBS) (ATCC), at 37 °C with 5% CO_2. The medium was refreshed every 2–3 days. For EIS measurements, the cells were harvested by centrifuging at 1200 rpm for 5 min. The supernatant fluid was disposed and the cells were resuspended in PBS buffer (Hyclone®) with a final concentration of ~100 μl^{-1}.

2.3. Cell capture on working electrode

The Au working electrodes were rinsed thoroughly with acetone, isopropanol, and dH_2O in series, followed by drying under N_2 gas flow. Optionally, the electrodes were under the sonication in ethanol for 2 min. After the cleaning, the devices were soaked in the freshly prepared mixture of 25 mM 11-mercaptoundecanoic acid (MUA) (Sigma–Aldrich, Co.) and 25 mM 3-mercaptopropionic acid (MPA) (Sigma–Aldrich, Co.) in ethanol (MUA:MPA = 1:10, v/v) for 15 h at room temperature. The working electrodes were rinsed with acetone and dried under N_2 gas flow. The electrodes were then soaked in an aqueous solution of 100 mM *N*-(3-dimethylaminopropyl)-*N*′-ethylcarbodiimide hydrochloride (EDAC) (Sigma–Aldrich, Co.)

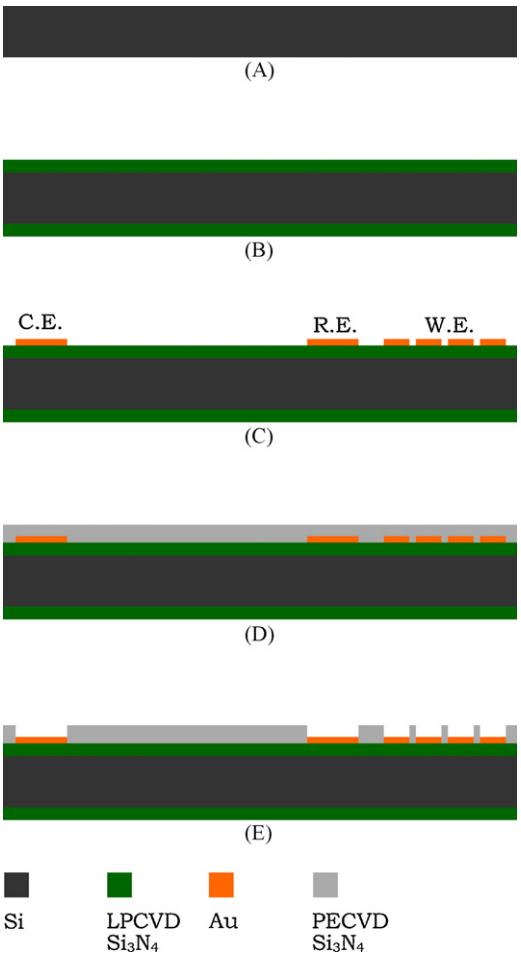

Fig. 1. Fabrication of $CD4^+$ cell biosensor. (A) A Si substrate. (B) The Si substrate deposited with a 300-nm thick LPCVD Si_3N_4 film. (C) The three-electrode system by a patterned deposition of 200-nm thick Au film, consisting of a counter electrode (C.E.), a reference electrode (R.E.), and an array of working electrodes (R.E.). (D) The surface passivation by depositing a 2-μm thick PECVD Si_3N_4 layer. (E) The Si_3N_4 removal on the top of the electrodes by CF_4 reactive ion etch.

and 25 mM *N*-hydroxysulfosuccinimide sodium salt (sulfo-NHS) (Sigma–Aldrich, Co.) for 1 h at room temperature. After rinsing with dH_2O, 1 μl of 0.5 μg μl^{-1} anti-human $CD4^+$ antibody (BD Biosciences, Inc.) was applied on the array of working electrodes and incubated at room temperature for 1 h. Afterwards, the working electrodes were rinsed with PBS buffer, followed by applying 1 μl of 0.1% bovine serum albumin (BSA) solution (Sigma–Aldrich, Co.) and incubating at room temperature for 1 h. After rinsing the electrodes with PBS buffer carefully, the J45.01 cells were applied on the working electrodes and left at room temperature for 30 min. The excessive cells were removed by dipping the electrodes in PBS buffer carefully. The devices were then ready for the EIS measurements.

2.4. Electrochemical impedance spectroscopy

The cells were detected by measuring the electrochemical impedance spectrum changes introduced by the cell attachment. The impedance measurements were taken under the three-electrode mode in the aqueous phase. The counter electrode, the reference electrode, and the cell-coated working electrode were connected through PBS buffer. A polydimethylsiloxane (PDMS) sheet patterned with an open window was placed on the sensor device to serve as a buffer container. The window was aligned with the array of the working electrode in the chip center. The three types of electrodes were within the window, being exposed to air. PBS buffer was added into the window, connecting the three electrodes. Another PDMS sheet was then placed on the top of the previous one, covering the window completely. This second PDMS layer was for preventing the evaporation of the PBS buffer. With this encapsulation, the device was able to last for hours without drying.

The impedance spectra of the working electrode pixels at the following stages were also measured for the characterization purpose: (1) the unmodified electrodes, (2) the electrodes after the MUA/MPA treatment, (3) the electrodes after the sulfo-NHS/EDAC treatment and (4) the electrodes after the antibody attachment.

The instrument used for the EIS measurements was FAS2 Femtostat from Gamry, Inc. The measurements were operated by the Gamry software "Framework" version.4.35. The impedance data were analyzed using the Gamry software "Echem Analyst" Version.1.35. The sweeping frequency range was 0.1 Hz to 300 kHz. The applied ac voltage was 10 mV. The dc bias was set to be 0 V relative to the open circuit potential. The initial delay for the system stabilization was set to be 100 s. Impedance data were collected 10 points per decade of the frequency. The measurements were performed at room temperature with minimized vibration noise.

3. Results and discussion

Fig. 2(A) shows the CAD of the biosensor chip. The overall chip size was 1.4 cm × 1.4 cm. An array of 200 working electrodes was located in the center of the chip. The two rectangles near to the working electrodes were the reference electrodes, each having an area of 300 μm × 600 μm. Two sets of counter electrodes were located relatively far away from the working electrodes. One set was aligned with the center horizontally and the other vertically. Each counter electrode had a surface area of 300 μm × 300 μm. At each corner were arranged 50 identical contact pads, connecting to 50 working electrodes in the center individually through 4-μm wide conduction lines. Each contact pad was 300 μm × 300 μm in size. The contact pads for the reference and counter electrodes were 500 μm × 500 μm each, connected to the corresponding electrodes through 20-μm wide lines. Fig. 2(B) is the image scanned for a realistic biosensor chip.

Fig. 2(C) is the optical images of the working electrodes located in the center of the chip. Each working electrode was 7 μm × 7 μm, with a gap of 2 μm between any adjacent electrodes. The electrode density was $\sim 10^4$ mm^{-2}. Since the diameter of $CD4^+$ cells was typically 8–10 μm, the size of the working electrodes was designed to be comparable to a single $CD4^+$ cell such that each working electrode would be able to capture one cell only. Therefore, the "on" or "off" state of each working electrode could be represented by the binary status of the cell occupancy on the electrode ("occupied" or "empty"). The 200 working electrodes were arranged in two lanes, each having 100 electrodes. The entire chip was deposited with a 2-μm thick Si_3N_4 layer to passivate all the connection lines. The Si_3N_4 on the top of the electrodes and the contact pads were removed by the CF_4 plasma etch. The opening windows were identical to the electrodes in size. The three electrodes were connected through PBS buffer. All the connection lines were covered with the 2-μm thick Si_3N_4 layer, being insulated from PBS buffer.

The working electrode pixels were modified with $CD4^+$ antibodies through three steps of chemical crosslinkings. First, the Au surface was modified with the carboxyl-terminated MUA/MPA through the Au-thiol affinitive binding. MUA/MPA was sensitive to moisture, so the reagent needed to be prepared freshly every time prior to the experiment. Second, with the presence of EDAC, sulfo-NHS reacted with the carboxyl group on MUA/MPA, forming a carboxylate intermediate. In the last, $CD4^+$ antibodies were

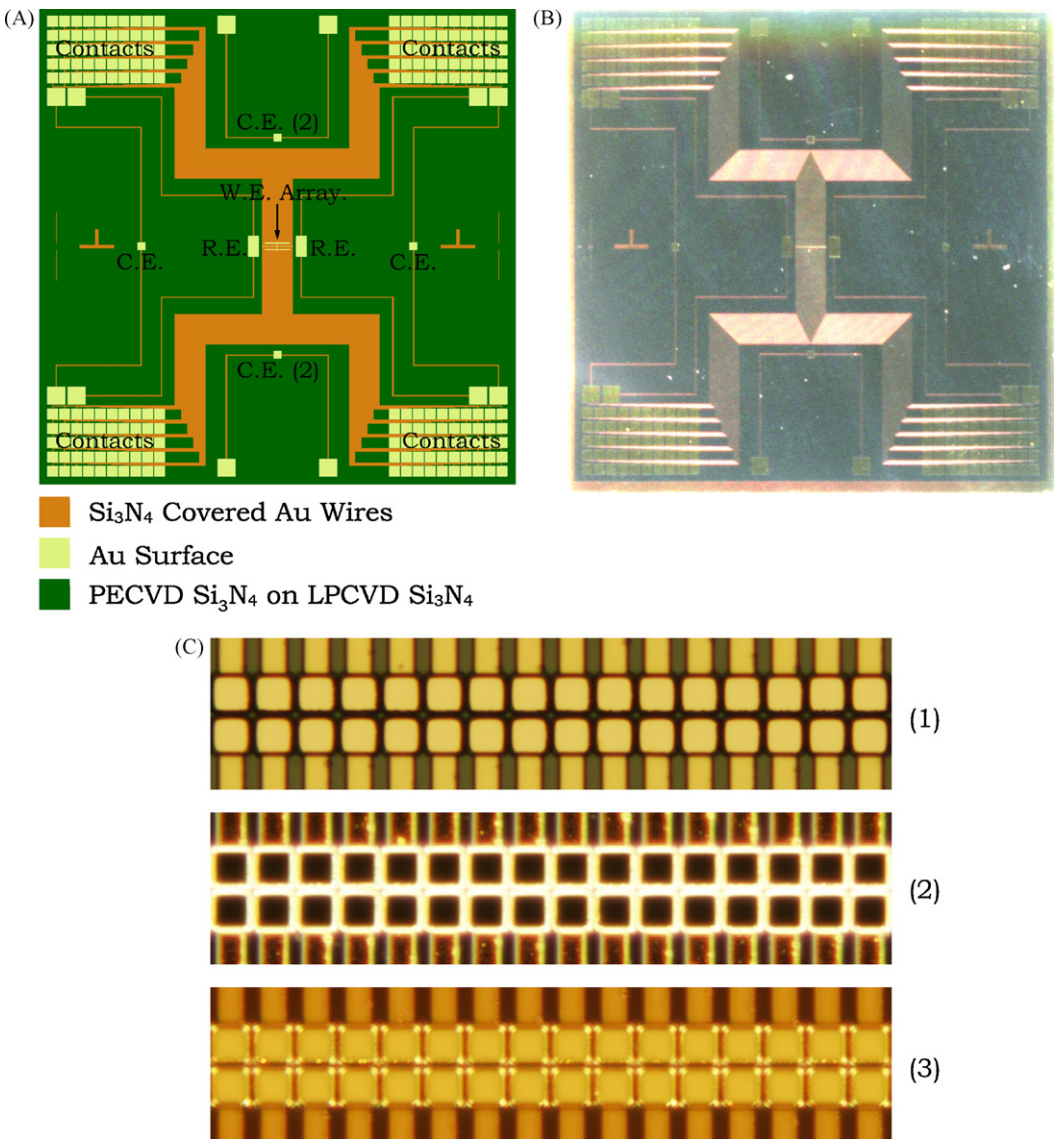

Fig. 2. Top view of $CD4^+$ cell biosensor. (A) The CAD of the biosensor chip. 200 working electrodes (W.E.) were located in the chip center, each of which was connected to a contact pad at the corner. Reference electrodes (R.E.) were close to the W.E. array whereas the counter electrodes (C.E.) were far away from the center. A second set of C.E. was added for optional use. (B) An image scanned from a realistic biosensor chip. (C) The optical images of the W.E. array under the bright-field (1), dark-field (2), and DIC mode (3). Each working electrode was 7 μm × 7 μm in size, with an interval distance of 9 μm. The black squares under mode 2 indicated that the working electrodes were flat and clean. In mode 3, the connection lines and the squares showed different colors, suggesting that the PECVD Si_3N_4 on the top of the working electrodes had been removed by the CF_4 dry etch.

attached to the MUA/MPA by replacing the sulfo-NHS in the carboxylate intermediate. The working electrodes were rinsed with PBS buffer and applied with 1 μl of 0.1% BSA solution for 1 h to minimize the non-specific binding sites. 1 μl of J45.01 cells with a concentration of $\sim 100\,\mu l^{-1}$ was applied on the antibody-coated working electrodes for 30 min at the room temperature. The $CD4^+$ antibodies selectively captured the J45.01 cells through the antibody–antigen recognition. The electrodes were slowly immersed in PBS buffer to rinse off the cell solution. The working electrodes coated with the J45.01 cells were inspected under microscope in the dark-field mode, shown in Fig. 3(A). In the image, each dark square was a single working electrode in the "off" state (no cell attached), whereas each bright spot was an electrode in the "on" state (attached with one single J45.01 cell on the surface). Using such densely packed electrode pixels had two great advantages: first, as the pixel size was comparable to a single $CD4^+$ cell, each electrode pixel could capture either one cell or none, therefore achieving a single-cell detection resolution. The detection error of each electrode pixel was minimized by the high signal-to-background ratio in this binary detection mode. Second, the entire sensing area was composed of individual electrode pixels. Each cell in the sensing area was sensed by a local pixel independently. Therefore the overall counting accuracy was in principle independent from the cell concentration and the distribution uniformity. It made this counting method robust for a wide range of the cell sample conditions and the capture characteristics. The capture selectivity was proven by the control experiment in which Farage cells ($CD19^+$) were applied on the electrodes modified with $CD4^+$ antibodies. Since there were no specific bindings between $CD19^+$ cells and $CD4^+$ antibodies, the cells were not captured on the electrodes, shown as Fig. 3(B).

As the image shows, all the captured cells were well located in the center of the working electrode. The success of this precise alignment was primarily due to the surrounding Si_3N_4 layer. The Si_3N_4 grid between adjacent electrodes served as 2-μm tall bounding walls, which was crucial for centering the cells on the electrodes

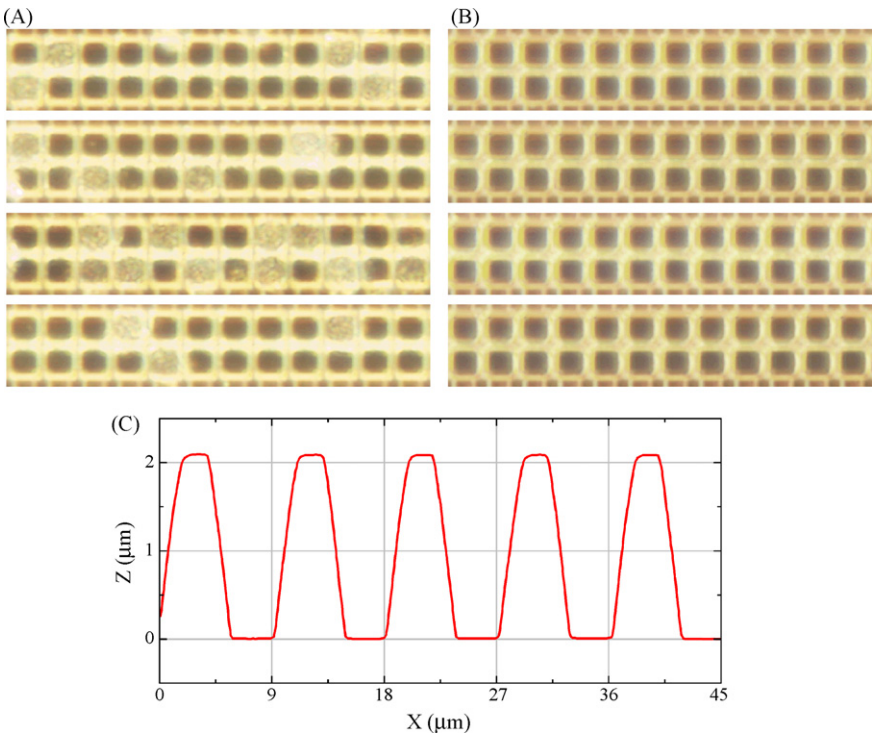

Fig. 3. Cell capture on CD4⁺ cell biosensor. (A) The working electrodes captured with CD4⁺ cells. The image was taken under the dark-field mode, showing the electrodes captured with a single cell on the surface (bright spots), as well as the electrodes with no cells captured (dark spots). The on-and-off state of the working electrodes was clearly represented by the binary status of the cell occupancy. (B) The working electrodes after coating with Farage (CD19⁺) cells. Since there were no specific bindings between CD19⁺ cells and CD4⁺ antibodies, CD19⁺ cells were not captured on the CD4⁺-antibody-modified electrodes. (C) The cross-sectional profile scanned across a few empty working electrode pixels, showing the 2-μm high PECVD Si_3N_4 grid structure between adjacent electrode pixels. Because of this grid structure, all the captured cells were well centered on the working electrodes.

when the cells landed on the surface. This aligned attachment was important for achieving the binary state of the cell occupancy. Fig. 3(C) is the surface profile across a few empty working electrodes, scanned by a profilometer. It clearly showed the periodic Si_3N_4 grid structure.

The impedance spectrum of a blank sensor device, as well as that after each step of the surface modifications, was measured in PBS buffer, within a frequency range from 0.1 Hz to 300 kHz. The recorded spectra are displayed in Fig. 4. The overall impedance spectra had an approximately linear dependence upon the frequency in the log–log Bode plot, ranging from $\sim 10^{10}\ \Omega$ at the low-frequency end to $\sim 10^{4}\ \Omega$ at the high-frequency end. The associated phase angles (θ) were less than -70°, suggesting that the total impedances were dominated by the capacitive component(s) in the circuit, caused by the electric double layer in the vicinity of the electrode surface.

As seen from the figure, the impedance spectra before and after the electrode was attached with a single J45.01 cell were significantly different. The total impedance (Z) increased by $\sim 10^{10}\ \Omega$ at the low-frequency end (0.1 Hz), suggesting that the presence of the single cell on the electrode posed a significant resistance to the current passage at the low-frequency end. The changes of the low-frequency impedance between earlier surface modification steps (steps 1–5) were noticeable. After the Au electrode was coated with MPA/MUA, Z at 0.1 Hz decreased by $2.58 \times 10^{9}\ \Omega$, indicating that the MPA/MUA film facilitated the interfacial charge transport possibly because of the hydrophilic carboxyl (–COOH) terminals. The subsequent modification with sulfo-NHS and EDAC increased Z by $3.88 \times 10^{9}\ \Omega$. After the CD4⁺ antibodies were attached Z decreased by $4.13 \times 10^{9}\ \Omega$. The impedance change caused by the further coating with BSA proteins was small ($2.56 \times 10^{8}\ \Omega$). Upon the cell capture, the impedance increase was large ($\sim 10^{10}\ \Omega$) and consistent, being able to explicitly distinguish the "on" and "off" states of

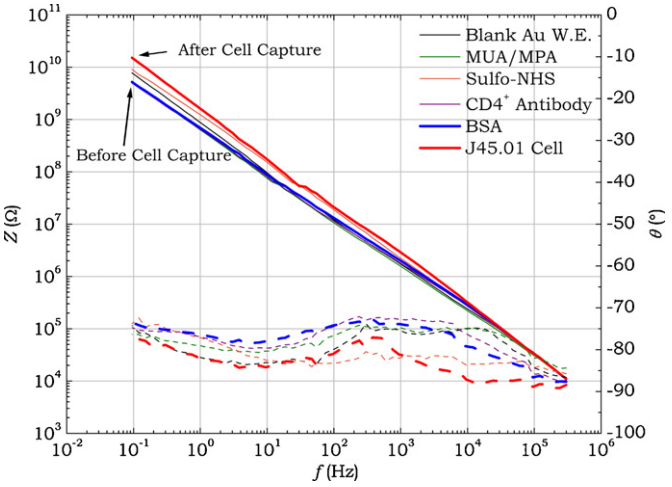

Fig. 4. Impedance spectra of CD4⁺ cell biosensor. The frequency (f) spectrum of the impedance (Z) (solid) and the corresponding phase angle (θ) (dashed) of a working electrode with: no chemical modifications (black), MUA/MPA monolayer (green), sulfo-NHS coating (yellow), CD4⁺ antibody attachment (purple), BSA blocking (blue), and cell capture (red). The impedance increase upon the cell capture was significant at the low-frequency end (0.1 Hz). (For interpretation of the references to color in this figure caption, the reader is referred to the web version of the article.)

the working electrode. Therefore the impedance data at single frequency point (0.1 Hz) were used for the analysis of the cell detection and counting.

Fig. 5(A) shows the histogram of Z at 0.1 Hz obtained from 30 identical working electrodes. On the left side was the impedances measured on the electrodes that were coated with CD4⁺ antibodies and BSA proteins, ranging from $3 \times 10^{9}\ \Omega$ to $10 \times 10^{9}\ \Omega$. The bars on the right side, ranging from $1.2 \times 10^{10}\ \Omega$ to $2.2 \times 10^{10}\ \Omega$,

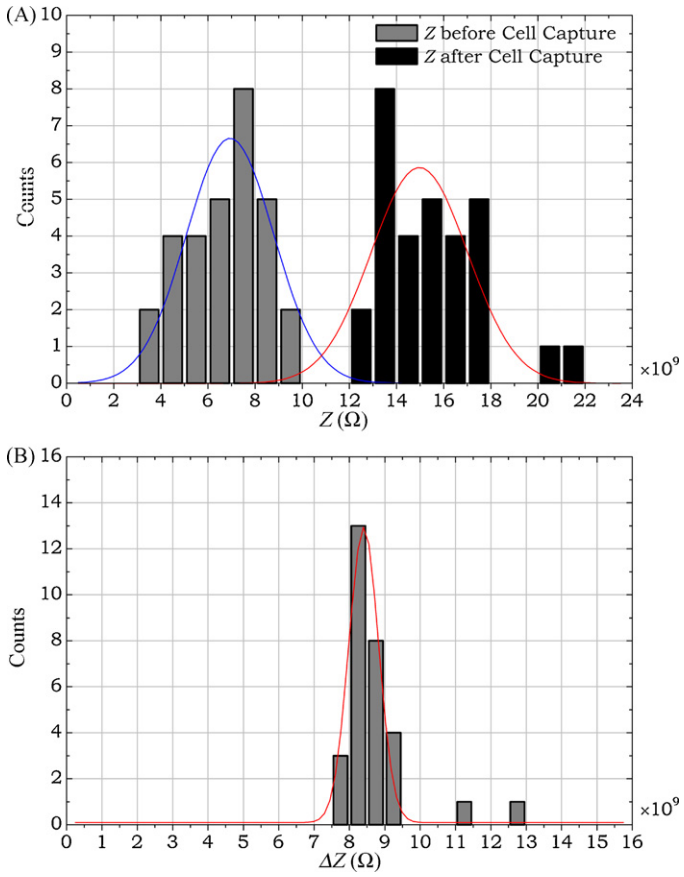

Fig. 5. (A) Impedances before and after cell capture. The gray columns show the distribution of the total impedance (Z) measured from 30 working electrode pixels before the cell capture (mean: $6.94 \times 10^9\ \Omega$; σ: $1.86 \times 10^9\ \Omega$). The black columns show the corresponding distribution after the cell capture (mean: $1.50 \times 10^{10}\ \Omega$; σ: $2.05 \times 10^9\ \Omega$). (B) Impedance change by cell capture. The histogram shows the distribution of the impedance change (ΔZ) introduced by the cell capture (mean: $8.40 \times 10^9\ \Omega$; σ: $4.18 \times 10^8\ \Omega$). The data were measured from 30 working electrode pixels.

were measured from the same electrodes after they each were attached with a single cell. The two groups of data were located with a significant separation distance, representing the "empty" and "occupied" states, respectively. Fig. 5(B) shows the distribution of the impedance change (ΔZ) caused by the cell attachment. The majority of the impedance changes fell in a narrow range, from $7.5 \times 10^9\ \Omega$ to $9.5 \times 10^9\ \Omega$. Therefore a value of $5 \times 10^9\ \Omega$ could serve as a reasonable threshold point for determining the binary status of the cell occupancy on the electrode.

In this biosensor, the cell counting was essentially digitalized. The total amount of the J45.01 cells captured by the electrode array was simply the sum of the electrode pixels in the "on" state. To verify the correlation between the impedance signals and the cell occupancies, the electrode array after the cell capture was inspected optically. The electrodes attached with cells were counted manually under microscope. Fig. 6 is the comparison between the optical enumeration and the impedance detection. The linear relationship demonstrated the single-cell detection resolution and the accurate cell counting by the use of the pixelated working electrodes.

The novelty of this biosensor was the digitalization of the cell counting by using pixelated electrodes. The counting was in principle independent of the cell population. As demonstrated, it precisely enumerated a low amount of $CD4^+$ cells. It could be useful for the quantitative clinical staging of HIV infection for AIDS patients. The device could also be used for diagnosing normal

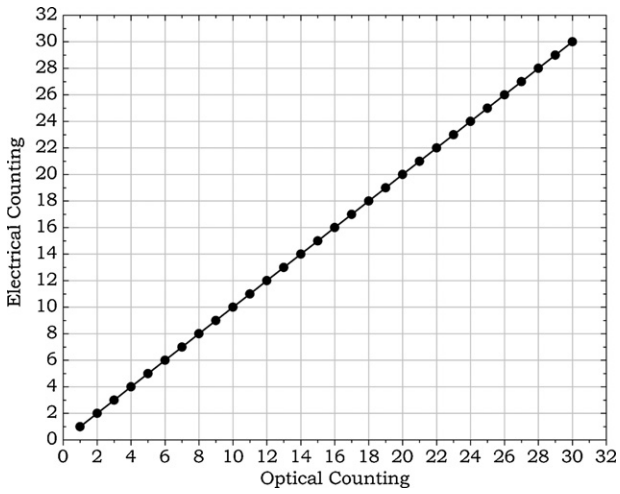

Fig. 6. Counting accuracy of $CD4^+$ cell biosensor. The plot shows a linear relation between the cells counted by the optical microscopy and the ones by the pixelated impedance sensor, demonstrating a single-cell detection resolution and an ideal counting accuracy from the pixelated impedance sensor. The threshold of the binary detection was set to be $5 \times 10^9\ \Omega$. Based on Fig. 5(B), the reading confidence was larger than 8σ.

people as well who have higher $CD4^+$ cell concentrations. Counting large number of cells would be possible for this biosensor by designing more electrode pixels on the chip or reducing the sample volume. In addition, as the sensor device demonstrated an excellent counting precision when the cell amount was low, handling large number of cells could also be worked out simply by using diluted samples. Being able to process diluted samples would be an attractive advantage in practice because it would require much less original samples. In this work the chemical modification was a general approach for immobilizing antibody proteins on gold surface, meaning that the device could be generalized to detect other types of immune targets by choosing an appropriate antibody–antigen pair and coating the corresponding antibodies on the electrode surface. The fabrication of the sensor device was simple, only containing two layers of processes. To reduce the fabrication cost, the Si/Si_3N_4 substrate could be substituted with cheaper materials such as glass. With the very-large-scale integration and the mass production, future practical devices could be expected to sufficiently inexpensive to be disposable.

4. Conclusion

A microchip biosensor based on electrochemical impedance spectroscopy has been developed for precise counting human $CD4^+$ lymphocyte cells. The key feature of the sensor device was an array of densely packed working electrode pixels. Each of them was as small as a single $CD4^+$ cell. These working electrodes were chemically modified with $CD4^+$ antibodies on the surface, being able to selectively capture one single $CD4^+$ cell on each electrode. A Si_3N_4 grid structure was built along with the working electrode pixels, playing an important role in aligning cells on the electrodes. The "on" and "off" states of each electrode pixel, depending on the cell capture status, was monitored by measuring the electrochemical impedance spectrum between the working and counter electrodes. The experimental data showed that the cell capture on an electrode pixel increased the interfacial impedance by at least $7 \times 10^9\ \Omega$. The cell counting by this pixelated electrode system agreed well with the optical counting. The impedance biosensor had a single-cell detection resolution while the counting precision was independent of the cell population. The binary detection mode digitalized the cell counting, making the system reliable and robust to environmental

noises. The device presented a new approach for the precise quantification of $CD4^+$ cells, oriented for future portable point-of-care tools for the HIV infection diagnosis.

Acknowledgements

This work was supported in part by the Nanobiotechnology Center (NBTC), an STC Program of the National Science Foundation under Agreement No. ECS-9876771. The device fabrication was done at Cornell NanoScale Science and Technology Facility (CNF), Ithaca, NY, USA. The Authors thank Thomas Zieziulewicz and David Lawrence at Wadsworth Center, Albany, NY, USA for their support in cell culture.

References

Alimonti, J.B., Ball, T.B., Fowke, K.R., 2003. J. Gen. Virol. 84, 1649–1661.
Centers for Disease Control, 1993. 1993 Revised Classification System for HIV Infection and Expanded Surveillance Case Definition for AIDS Among Adolescents and Adults.
Cheng, X.H., Irimia, D., Dixon, M., Sekine, K., Demirci, U., Zamir, L., Tompkins, R.G., Rodriguez, W., Toner, M., 2007a. Lab Chip 7 (2), 170–178.
Cheng, X.H., Irimia, D., Dixon, M., Ziperstein, J.C., Demirci, U., Zamir, L., Tompkins, R.G., Toner, M., Rodriguez, W.R., 2007b. J. AIDS 45 (3), 257–261.
Department of Health and Human Services, 2005. Guidelines for the Use of Antiretroviral Agents in Pediatric HIV Infection.
Feldman, C., 2005. Curr. Opin. Infect. Dis. 18 (2), 165–170.
Gottlieb, M.S., 2006. Am. J. Public Health 96 (6), 980–981, discussion 982–983.
Holmes, C.B., Losina, E., Walensky, R.P., Yazdanpanah, Y., Freedberg, K.A., 2003. Clin. Infect. Dis. 36 (5), 652–662.
Joint United Nations Programme on HIV/AIDS, 2008. 2008 Report on the Global AIDS Epidemic.
Jokerst, J.V., Floriano, P.N., Christodoulides, N., Simmons, G.W., McDevitt, J.T., 2008. Lab Chip 8 (12), 2079–2090.
Landay, A., Ohlssonwilhelm, B., Giorgi, J.V., 1990. AIDS 4 (6), 479–497.
Mishra, N.N., Retterer, S., Zieziulewicz, T.J., Isaacson, M., Szarowski, D., Mousseau, D.E., Lawrence, D.A., Turner, J.N., 2005. Biosens. Bioelectron. 21 (5), 696–704.
Rodriguez, W.R., Christodoulides, N., Floriano, P.N., Graham, S., Mohanty, S., Dixon, M., Hsiang, M., Peter, T., Zavahir, S., Thior, I., Romanovicz, D., Bernard, B., Goodey, A.P., Walker, B.D., McDevitt, J.T., 2005. PLos Med. 2 (7), 663–672.
Sepkowitz, K.A., 2001. New Eng. J. Med. 344 (23), 1764–1772.
Thorslund, S., Larsson, R., Bergquist, J., Nikolajeff, F., Sanchez, J., 2008. Biomed. Microdevices 10 (6), 851–857.
Thorslund, S., Larsson, R., Nikolajeff, F., Bergquist, J., Sanchez, J., 2007. Sens. Actuators B: Chem. 123 (2), 847–855.
Wang, Y.N., Kang, Y.J., Xu, D.Y., Chon, C.H., Barnett, L., Kalams, S.A., Li, D.Y., Li, D.Q., 2008. Lab Chip 8 (2), 309–315.
Weiss, R.A., 1993. Science 260 (5112), 1273–1279.